Official URL:

https://doi.org/10.1017/jfm.2019.662

Model for the dynamics of micro-bubbles in high-Reynolds-number flows

Zhentong Zhang[1]**, Dominique Legendre**[1] **and Rémi Zamansky**[1,†]

[1]Institut de Mécanique des Fluides de Toulouse (IMFT), Université de Toulouse, CNRS, INPT, UPS, Toulouse, France

We propose a model for the acceleration of micro-bubbles (smaller than the dissipative scale of the flow) subjected to the drag and fluid inertia forces in a homogeneous and isotropic turbulent flow. This model, that depends on the Stokes number, Reynolds number and the density ratio, reproduces the evolution of the acceleration variance as well as the relative importance and alignment of the two forces as observed from direct numerical simulations (DNS). We also report that the bubble acceleration statistics conditioned on the local kinetic energy dissipation rate are invariant with the Stokes number and the dissipation rate. Based on this observation, we propose a stochastic model for the instantaneous bubble acceleration vector accounting for the small-scale intermittency of the turbulent flows. The norm of the bubble acceleration is obtained by modelling the dissipation rate along the bubble trajectory from a log-normal stochastic process, whereas its orientation is given by two coupled random walks on a unit sphere in order to model the evolution of the joint orientation of the drag and inertia forces acting on the bubble. Furthermore, the proposed stochastic model for the bubble acceleration is used in the context of large eddy simulations (LES) of turbulent flows laden with small bubbles. To account for the turbulent motion at scales smaller than the mesh resolution, we decompose the instantaneous bubble acceleration in its resolved and residual parts. The first part is given by the drag and fluid inertia forces computed from the resolved velocity field, and the second term refers to the random contribution of small unresolved turbulent scales and is estimated with the stochastic model proposed in the paper. Comparisons with DNS and standard LES, show that the proposed model improves significantly the statistics of the bubbly phase.

Key words: bubble dynamics, particle/fluid flow, isotropic turbulence

1. Introduction

In various industrial set-ups, such as chemical reactors, water treatment, steam generators and systems for drag reduction, the presence of a bubble phase plays an essential role. The further improvement of these applications rely on our ability to predict the dynamics of the bubbles in highly turbulent flows. However, even if the equation for the dynamics of micro-bubbles (i.e. bubbles smaller than the

dissipative scale of the flow) is well known and only depends on the local velocity of the fluid and its derivatives (Gatignol 1983; Maxey & Riley 1983; Magnaudet & Eames 2000), it remains challenging to precisely estimate the statistics of the bubble acceleration in turbulent flows. These difficulties arise because all the flow scales affect the bubble motion. In particular, the small scales of the flow play an essential role. Indeed, for small bubbles, the dominance of the fluid inertia term in the bubble dynamics equation leads to an increase of the bubble acceleration variance with the bubble diameter (Calzavarini *et al.* 2009; Prakash *et al.* 2012; Mathai *et al.* 2016) in contrast with inertial particles for which the fluid inertia terms can be neglected. Further, the non-Gaussian acceleration probability density functions (p.d.f.s) with broad probability tails of high bubble acceleration events observed experimentally and numerically (Mazzitelli & Lohse 2004; Volk *et al.* 2008*a*; Prakash *et al.* 2012) stress the importance of the intermittent fluctuations characteristic of the small scales of the flow. In addition, the specificity of bubble acceleration statistics has been shown to affect, among other important statistical quantities, their dispersion and clustering properties (Mazzitelli & Lohse 2004; Calzavarini *et al.* 2008; Tagawa *et al.* 2012, 2013).

For very large Reynolds-number flows, it remains impossible to resolve all the turbulent scales with direct numerical simulations (DNS). This is why, when the large scale features of the flow mainly depend on the specific configuration, the large eddy simulations (LES) approach is commonly used. In such approaches, the effective action of the small-scale motions on the large-scale evolution is parameterized. Models based on the turbulent viscosity have proved to reasonably achieve such parameterization of the energy transfer rate below the resolved scale (Meneveau & Katz 2000; Sagaut 2002). Following this procedure, one obtains the evolution of a coarse-grained filtered velocity field, $\bar{u}_f$. Within this framework, the standard approach to perform LES with Lagrangian tracking for the dispersion of micro-bubbles in a turbulent flow is to substitute the local fluid velocity by the filtered velocity field in the bubble dynamics equation (Climent & Magnaudet 1999; van den Hengel, Deen & Kuipers 2005; Hu & Celik 2008; Dhotre *et al.* 2013). However, doing so, the small (unresolved) scales of the flow are discarded from the bubble dynamics, resulting in strong underestimation of the bubble acceleration.

Different approaches were considered to account for the unresolved scales in the calculation of the drag force on small inertial particles. Most of them rely on the stochastic estimation of the subgrid fluid velocity along the Lagrangian trajectory of the particles (Fede & Simonin 2006; Berrouk *et al.* 2007; Pozorski & Apte 2009; Minier, Chibbaro & Pope 2014; Breuer & Hoppe 2017; Johnson & Meneveau 2017; Sawford 1991; Sawford & Guest 1991; Park *et al.* 2017). Nevertheless, none of these approaches addressed the issue of the fluid inertia force, which is essential for bubble dynamics. Aside, approaches have been proposed to reconstruct the fluid fluctuations in the Eulerian fields which can in turn be used to advect the dispersed phase (Kerstein 1999; Burton & Dahm 2005*a*,*b*; Ghate & Lele 2017). Among them Sabel'nikov, Chtab & Gorokhovski (2007) introduced the decomposition of the instantaneous fluid acceleration field into a filtered contribution and a random contribution to account for the intermittency at small, unresolved, scales (see also Sabel'nikov, Chtab-Desportes & Gorokhovski 2011; Zamansky, Vinkovic & Gorokhovski 2013; Sabelnikov, Barge & Gorokhovski 2019). Recently, Gorokhovski & Zamansky (2018) considered a similar decomposition for the instantaneous acceleration of dispersed objects,

$$\boldsymbol{a}_b = \underbrace{\bar{\boldsymbol{a}}_b}_{\substack{\text{large-scale} \\ \text{contribution}}} + \underbrace{\boldsymbol{a}_b^*}_{\substack{\text{small-scale random} \\ \text{contribution}}} . \tag{1.1}$$

The temporally and spatially filtered force is obtained from the resolved velocity field, $\overline{u}_f$, while the random force accounts for fluctuations at unresolved scales. The filtered contribution presents much less intense fluctuations than the total acceleration as can be verified in Lalescu & Wilczek (2018). In line with the Kolmogorov hypothesis, it is assumed that the main source of randomness in the acceleration is attributed to the fluctuation of the local energy transfer rate. We then propose to approximate the instantaneous small scale contribution of the acceleration by the acceleration conditionally averaged on the local value of the dissipation rate as 'seen' along the Lagrangian path $\varepsilon_* : \boldsymbol{a}_b^* \approx \langle \boldsymbol{a}_b \mid \varepsilon_* \rangle$. Within the LES framework, ε_* has to be modelled since its wide fluctuations cannot be resolved from the filtered velocity field. For solid inertial particles solely subject to the Stokes drag force, Gorokhovski & Zamansky (2018) proposed such a model along with a log-normal stochastic process as a surrogate to the local dissipation rate. In the present paper, we extend this approach to the dynamics of micro-bubbles dispersed in turbulent flows. We first use DNS to analyse the statistics of the bubble acceleration and of the two main forces acting on the bubble (drag and fluid inertia forces). Specifically, we investigate the evolution of the magnitude of the two forces with the bubble diameter and their relative orientation, as well as the statistics of the bubble acceleration conditioned on the local dissipation rate. To estimate the magnitude of the acceleration, we propose a model based on the bubble spectral response to the fluid velocity fluctuation initially proposed by Tchen (1947). Further, consistently with the time scale separation between the evolution of the norm and the orientation (Pope 1990; Mordant, Crawford & Bodenschatz 2004), our modelling is supplemented with a stochastic process for the orientation, $\boldsymbol{a}_b^* = |a^*|\boldsymbol{e}^*$. The proposed model accounts for intermittency effects, as well as the correlation and alignment between the drag force and the fluid inertia force.

The outline of the paper is as follows: in §2 we provide the numerical details of the DNS and the LES of statistically stationary homogeneous and isotropic turbulent flows. In §3, we report the statistics of the acceleration and of the forces obtained from the DNS for various Stokes numbers. We also present a model describing the dependence of these statistics. Section 4 gives the formulation of the stochastic models accounting for the unresolved fluid acceleration. Subsequently the coupling of this model with LES is assessed by comparison with DNS and standard LES.

2. Details of the numerical simulations

We consider very small bubbles dispersed in an isotropic homogeneous turbulent flow. The continuous liquid phase is given by the incompressible Navier–Stokes equation and the dispersed phase is treated with a point particle approach. The feedback of the bubbles on the carrier phase is disregarded. The carrier flow field is computed with a pseudo-spectral method in a periodic box (Zamansky *et al.* 2016; Gorokhovski & Zamansky 2018; Bos & Zamansky 2019). In order to maintain a statistically stationary state, a forcing term active at the smallest wavenumbers is applied to the Navier–Stokes equation (Chen *et al.* 1993). The flow field is simulated by DNS and LES for the same Reynolds number, and the details of the simulation parameters are given in table 1. For the LES, the turbulent viscosity is estimated by the standard Smagorinsky model, $\nu_\Delta = C_s \Delta |\overline{S_{ij}}|$, where $\overline{S_{ij}}$ is the filtered rate of strain tensor, Δ is the cutoff scale and C_s is the model parameter. With the Smagorinsky model, the energy transfer rate from scale Δ, $\varepsilon_\Delta = 2(\nu + \nu_\Delta)\overline{S_{ij}}\,\overline{S_{ij}}$ can give a relatively good estimate of the average energy flux, $\langle \varepsilon_\Delta \rangle = \langle \varepsilon \rangle$, with ε being the local rate of kinetic energy dissipation. However, the energy transfer rate from scale Δ typically

Method	N	Re_H	Re_λ	τ_L/τ_η	$\dfrac{\langle\varepsilon\rangle H}{K^{3/2}}$	L/η	η/Δ	ν_Δ/ν	τ_Δ/τ_η
DNS	1024^3	10 600	216	55.8	1.9	418	0.8	—	—
LES	64^3	10 100	193	51.3	2.09	367	0.045	9.7	52
LES	48^3	9 800	187	48.4	2.3	336	0.034	14.6	59
LES	32^3	9 381	175	45.5	2.47	307	0.02	25	80

TABLE 1. The numerical parameters of the DNS and LES. The number of grid points in each direction is given by N. The size of numerical domain is $H = 2\pi$, $\tau_L = (2/3K)/\varepsilon$ is the eddy turnover time, $L = (2/3K)^{3/2}/\varepsilon$ is the scale of the large eddies, K is the average turbulent kinetic energy and ε is the average dissipation rate. The Reynolds number based on the large scale of the flow is given by Re_H, Re_λ is Reynolds number based on the Taylor length scale, η and τ_η are the Kolmogorov length and time scale and $\tau_\Delta = \Delta^2/\nu_\Delta$.

presents much less intense fluctuations compared to ε when $\Delta \gg \eta$. In the following, it is shown that ε is able to characterize the bubble dynamics, and we use a stochastic process to estimate the value of ε from ε_Δ.

For micro-bubbles in turbulence, the bubble equation of motion is essentially given by the drag force and the inertia force (Gatignol 1983; Maxey & Riley 1983; Magnaudet & Eames 2000),

$$\boldsymbol{a}_b(t) = \frac{\mathrm{d}\boldsymbol{u}_b(t)}{\mathrm{d}t} = -\frac{\boldsymbol{u}_b(t) - \boldsymbol{u}_f(\boldsymbol{x} = \boldsymbol{x}_b(t), t)}{\tau_b} + \beta \frac{\mathrm{D}\boldsymbol{u}_f}{\mathrm{D}t}(\boldsymbol{x} = \boldsymbol{x}_b(t), t); \quad \frac{\mathrm{d}\boldsymbol{x}_b(t)}{\mathrm{d}t} = \boldsymbol{u}_b(t),$$

$$(2.1a,b)$$

where $\boldsymbol{a}_b$, $\boldsymbol{u}_b$ and $\boldsymbol{x}_b$ are the bubble acceleration, velocity and position, $\boldsymbol{u}_f$ is the fluid velocity field and $\mathrm{D}\boldsymbol{u}_f/\mathrm{D}t = \partial\boldsymbol{u}_f/\partial t + \boldsymbol{u}_f \cdot \nabla\boldsymbol{u}_f$ is its material derivative. The parameter β, which compares the mass accelerated by the fluid to the mass accelerated by the bubble, is defined as $\beta = (1 + C_m)/(\Gamma + C_m)$, where Γ is the density ratio and C_m is the added mass coefficient ($C_m = 1/2$ for a sphere in an unbounded environment). For a bubble $\tau_b = d_b^2/(24\nu)$, with ν the kinematic viscosity and d_b the bubble diameter, and $\beta = 3$, assuming that the gas–liquid density ratio is vanishing, and that the bubbles are non-deformable spheres with free slip at the liquid interface. For a solid body with no slip at the interface one has $\tau_b = (\Gamma + C_m)d_b^2/(18\nu)$ and for large density ratio $\beta \approx 0$. In (2.1) the history and lift forces are discarded as they appear less important (Legendre & Magnaudet 1997, 1998; Magnaudet & Eames 2000; Mazzitelli, Lohse & Toschi 2003; Calzavarini et al. 2008). Also as shown by Mathai et al. (2016) the effect of gravity is negligible on the bubble dynamics as long as $St/Fr \ll 1$, with $St = \tau_b/\tau_\eta$ and $Fr = a_\eta/g$ being the Stokes and Froude numbers, respectively, $\tau_\eta = \sqrt{\nu/\langle\varepsilon\rangle}$ and $a_\eta = \sqrt{\langle\varepsilon\rangle/\tau_\eta}$ being the Kolmogorov time and acceleration scales, respectively. To evaluate the right-hand side of (2.1) the value of fluid velocity and total acceleration fields at the bubble positions are interpolated from the computational grid with the Hermite interpolation scheme. For each Stokes number we track 1 628 000 bubbles per Stokes number for the DNS and 62 800 for the LES. In table 2 we give the Stokes number for our seven sets of simulations. For a bubble with $\Gamma = 0$, the only possibility to vary the Stokes number is to change d_b/η through the relation $d_b/\eta = \sqrt{24St}$. As apparent, for the largest Stokes numbers considered here, the point particles approach appear unrealistic as $d_b/\eta > 1$. Note, however, that according to Calzavarini et al. (2009), the finite volume effects appear to be significant for $d_b/\eta > 10$. Moreover, as seen in table 2 for the largest Stokes numbers, the bubble Reynolds number, $Re_b =$

St	0.021	0.074	0.20	0.45	1.01	1.55	2.07
$d_b\eta$	0.70	1.33	2.19	3.29	4.93	6.10	7.04
Re_b	0.06	0.36	1.4	4.2	11.3	18.4	25.1

TABLE 2. The Stokes numbers and non-dimensional diameters of the bubbles used for the DNS and LES, and the bubble Reynolds numbers computed from the DNS.

$\sqrt{\langle(\boldsymbol{u}_f - \boldsymbol{u}_b)^2\rangle}d_b/\nu$, becomes significant, and the Stokes drag law is not strictly valid for those Stokes numbers. Nevertheless, the drag of a spherical clean bubble needs corrected by a function of Re ranging between 1 and 3 in the limit of infinite Reynolds number. Typically for the maximum value reported in table 2, the correction is 1.9. So we do not expect a qualitative change on the behaviour of the results presented below. Therefore, we choose to keep a simple drag law in order to simplify the analysis. Finally let us mention that from a dimensional point of view to have $St = 1$ and $Fr = 1$ for bubbles in water, with normal gravity ($g = 9.81$ m s^{-2}), requires $d_b \approx 0.0002$ m and $\varepsilon \approx 0.2$ m^2 s^{-3}.

The DNS results are detailed in the next section. They will serve as the basis for the discussion of the stochastic modelling developed in §4.

3. Statistics of the bubble acceleration and of the fluid forces on the bubbles

Response of small bubbles and particles to turbulence is known to depend on both Stokes number and β. This is illustrated in figure 1 which presents the normalized acceleration variance against the Stokes number for various value of β. In this figure we report the data obtained from our DNS for micro-bubbles ($\beta = 3$), the DNS for Calzavarini et al. (2009) for light particles ($\beta = 2.5$) and heavy particles ($\beta = 0.14$) and the DNS of Bec et al. (2010) for heavy particles ($\beta = 0$). For the heavy particles ($\beta < 1$), it is observed that the acceleration variance decreases when the Stokes number increases. This is in contrast to the case of bubbles and light particles ($\beta > 1$) in which the bubble normalized acceleration variance increases with St.

Based on the dynamics of the bubble given by (2.1) and following the approach of Tchen (1947) (see also Hinze 1975), one can derive a response function of the bubble velocity fluctuations to the fluid fluctuations, $H_u(\omega)$,

$$E_b(\omega) = H_u^2(\omega)E_f(\omega); \quad H_u^2(\omega) = \frac{1 + \beta^2\omega^2\tau_b^2}{1 + \omega^2\tau_b^2}, \quad (3.1a,b)$$

with ω the pulsation, and where $E_b(\omega) = \hat{\boldsymbol{u}}_b(\omega)\hat{\boldsymbol{u}}_b(-\omega)$ and $E_f(\omega) = \hat{\boldsymbol{u}}_f(\omega)\hat{\boldsymbol{u}}_f(-\omega)$ are the Lagrangian spectra of the bubble and fluid velocity and circumflexes are used to denote the Fourier coefficients. To obtain this relation we assume that the trajectory of the bubble does not deviate significantly from the trajectory of a fluid element as we substitute the material derivative of the fluid velocity by its time derivative along the bubble trajectory. This assumption is questionable as soon as the Stokes number of the bubble is not vanishingly small, and will be discussed later. Anyway, it enables us to easily obtain the qualitative behaviour of the bubble dynamics since in that case, it is not explicitly dependent on the fluid velocity gradient. As shown in the inset of figure 1, the response function differs significantly for a bubble ($\beta = 3$) and a heavy particle ($\beta = 0$). While for $\beta = 0$, the inertia of the particle filters the high frequency fluctuations of the fluid, for a bubble the high frequency fluctuations
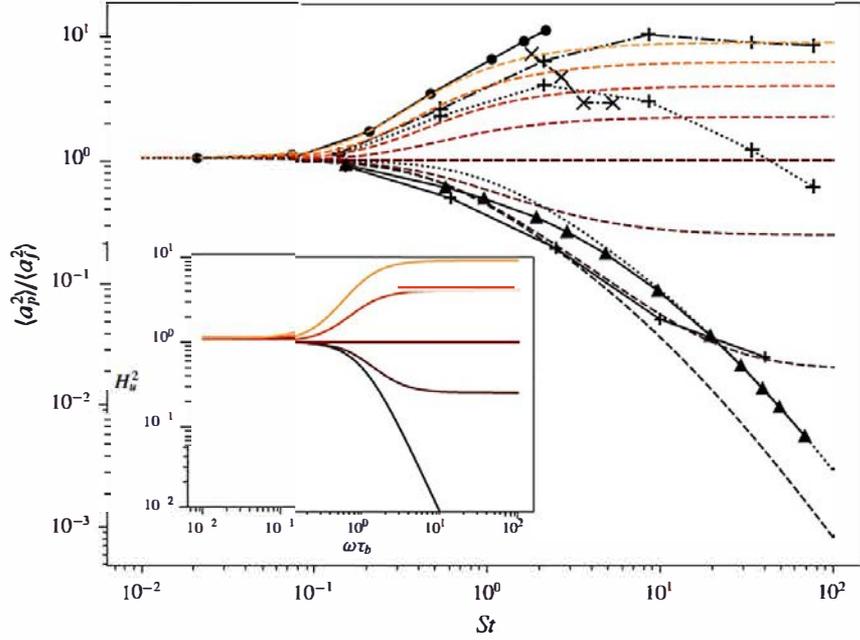
FIGURE 1. (Colour online) Acceleration variance normalized by the fluid tracer acceleration variance from our DNS for bubbles ($\bullet$ and continuous line), the DNS data of Bec *et al.* (2010) and Lanotte (2011) for heavy inertial particles $\beta = 0$, $Re_\lambda = 400$ ($\blacktriangle$ and continuous line), the DNS from Calzavarini *et al.* (2009) for $\beta = 2.5$ and $Re_\lambda = 180$, with and without the Faxén correction (+ with dotted and dot-dashed lines, respectively), and $\beta = 0.14$ (+ with continuous line), the experimental measurements from Prakash (2013) for $Re_\lambda = 145 - 230$ and $\beta \approx 3$ ($\times$ with dashed lines). Comparison with the relation (3.4), $\langle a_b^2 \rangle (St, \beta, Re_0)/\langle a_b^2 \rangle (0, 1, Re_0)$ with $c_1 = 2.8$ and $Re_0^{1/2} = 0.08 Re_\lambda = 16$ for $\beta = 0$, 0.14, 0.5, 1, 1.5, 2, 2.5 and 3 from black to orange, in dashed lines, and with $c_1 = 2.8$ and $Re_0^{1/2} = 0.08 Re_\lambda = 32$, $\beta = 0$ in black dotted line. The inset is the response function (3.1) as a function of $\omega \tau_b$ for $\beta = 0$, 0.5, 1, 2 and 3 from black to orange, respectively.

of the fluid are amplified. From this relation one can also obtain the response function relating the bubble acceleration fluctuations to the fluid velocity fluctuations along the bubble trajectory, $H_a(\omega)$,

$$E_a(\omega) = H_-^2(\omega) E_f(\omega) \qquad H_-^2 = \omega^2 H_-^2(\omega) \tag{3.2a,b}$$

with E_a the Lagrangian spectrum of the bubble acceleration. The bubble acceleration variance is given by $\langle a_b^2 \rangle = 2 \int_0^\infty E_a(\omega) \, d\omega$. To compute the variance, one needs to prescribe the Lagrangian fluid velocity spectrum along the bubble trajectory. For a fluid tracer the Lagrangian spectrum presents a power law for intermediate frequencies, $E_f(\omega) \sim \langle \varepsilon \rangle \omega^{-2}$ (Tennekes & Lumley 1972; Yeung 2001). To account for finite Reynolds number effects, and to have a finite energy density for $\omega \to 0$ we consider the form for the Lagrangian spectra (Hinze 1975; Mordant, Metz & Michel 2001) as follows:

$$E_f(\omega) \approx \frac{k_0 \langle \varepsilon \rangle}{\omega^2 + \omega_0^2} \tag{3.3}$$

with k_0 a constant, and ω_0^{-1} the Lagrangian integral time scale. Note that the relation (3.3) gives, for the velocity Lagrangian autocorrelation, $\rho(\tau) = \exp(-\omega_0\tau)$. As shown by Sawford & Yeung (2011), one has $(\tau_\eta\omega_0)^{-1} = (\omega_\eta/\omega_0)/2\pi \approx 0.08Re_\lambda$, with $\omega_\eta = 2\pi/\tau_\eta$. For convenience we note in the following $Re_0^{1/2} = (\tau_\eta\omega_0)^{-1}$. Furthermore the normalizing condition of the spectra, $\langle u_f^2 \rangle = 2\int_0^\infty E_f(\omega)\,d\omega$, gives after integration $\langle u_f^2 \rangle = \pi k_0 \langle\varepsilon\rangle/\omega_0$ that imposes $k_0 = 2(\tau_L/\tau_\eta)(\omega_0/\omega_\eta) \approx 4(\tau_L/\tau_\eta)Re_\lambda^{-1}$ with $\tau_L = \langle u_f^2 \rangle/\langle\varepsilon\rangle$ the large eddy time scale. This constant is computed from the DNS to be $k_0 \approx 1.04$ (see table 1). As seen from figure 2(a), with $k_0 = 1.03$ and $\omega_0/\omega_\eta = 0.0092$, the relation (3.3) provides a very good estimation of E_f for the various Stokes number considered here, for $\omega \ll \omega_\eta$. Nevertheless, the high frequency part of the spectra, which presents dependence on the Stokes number, is not predicted correctly by (3.3), an increase in inertia leads to more energy at high frequency. Let us note that for $\beta > 0$ the previous integral only converges if $E_f(\omega)$ decreases fast enough at large ω. Therefore to ensure its convergence, the integral is truncated above $k_1\omega_\eta$, independently of the Stokes number. This gives for the bubble acceleration variance the following relation:

$$\langle a_b^2 \rangle \approx c_0 a_\eta^2 \left[\beta^2 + \frac{1-\beta^2}{1-St_0^2}\frac{\tan^{-1}(c_1 St)}{c_1 St} - \frac{1-\beta^2 St_0^2}{1-St_0^2}\frac{\tan^{-1}(c_1 Re_0^{1/2})}{c_1 Re_0^{1/2}} \right], \qquad (3.4)$$

with $c_1 = 2\pi k_1$, $c_0 = 4\pi k_1 k_0$ and $St_0 = St/Re_0^{1/2}$ a Stokes number based on the large eddy time scale. Note that the previous relation does not present singularities for $St_0 = 1$ since in this case the last two terms cancel. Also $\langle a_b^2 \rangle$ remains positive for all St, Re_0 and β. Nevertheless, the assumptions used to derive (3.4) are *a priori* satisfied for $Re_0 \gg St^2$ and $Re_0 \gg 1$, and in this limit (3.4) becomes

$$\langle a_b^2 \rangle \approx c_0 a_\eta^2 \left[\beta^2 + (1-\beta^2)\frac{\tan^{-1}(c_1 St)}{c_1 St} \right]. \qquad (3.5)$$

A similar relation is proposed by Zaichik & Alipchenkov (2011). Their derivation is based on the same approximation for the fluid acceleration and assumes the fluid velocity correlation in physical space that include a viscous cutoff at small scale contrary to the relation (3.3) used here. The relation (3.4) with $c_1 = 2.8$ and $Re_0^{1/2} = 16$ is plotted in figure 1 for various St and β. In this figure, the bubble acceleration variance is normalized by the acceleration variance of fluid tracers estimated from the model (3.4) by setting $St = 0$ and $\beta = 1$. It is seen that (3.4) is overall in good agreement with the DNS data sets for $\beta = 3$, 2.5, 0.14 and 0. The discrepancy between the DNS and relation (3.4) observed for the inertial particles around $St = 1$, is attributed to the preferential concentration of particles, since this effect is not accounted for in the model. For the inertial particles at $St \approx 0.5$ the model overestimates the acceleration by approximately 20 %. It is also observed that for $St > 1$, (3.4) underestimates the DNS when $\beta = 3$ and 2.5. Note also that the evolution of the acceleration variance with St and β given by the model (3.4) appears qualitatively similar to the DNS data presented by Volk *et al.* (2008a). As expected, the acceleration variance normalized by the acceleration variance of fluid tracer tends to unity when St goes to 0 for every value of β, indicating that bubbles with bubbles with extremely small diameter effectively behave as fluid tracers. According to (3.4) for $\beta = 0$, the decrease of the acceleration variance with the Stokes number presents the same scaling as the relation proposed by Gorokhovski & Zamansky (2018), namely $\langle a_b^2 \rangle/a_\eta^2 \approx 1$ for $St \ll 1$, $\langle a_b^2 \rangle/a_\eta^2 \sim St^{-1}$ for $1 \ll St \ll \sqrt{Re_0}$ and $\langle a_b^2 \rangle/a_\eta^2 \sim St^{-2}$ for $St \gg \sqrt{Re_0}$ and appears consistent with the relation proposed by Bec *et al.* (2006).

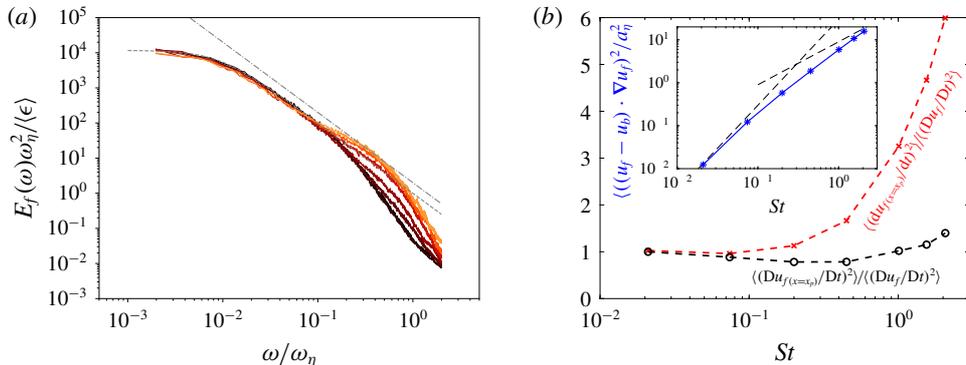FIGURE 2. (Colour online) (*a*) Lagrangian fluid velocity spectra along the bubble trajectory from the DNS for $St = 0.02$, 0.074, 0.20, 0.45, 1.01, 1.55 and 2.07 (from black to red, respectively). Comparison with the power law ω^{-2} and the relation (3.3), $k_0/((\omega/\omega_\eta)^2 + (\omega_0/\omega_\eta)^2)$ with $k_0 = 1$ and $\omega_0/\omega_\eta = 0.0092$ in grey dot-dashed and dashed lines, respectively. (*b*) Evolution with the Stokes number of the variance of the material derivative of fluid velocity at the bubble position (black circles) and of the Lagrangian time derivative along the bubble trajectories of the fluid velocity (red crosses). Both quantities are normalized by the global variance of the fluid tracer acceleration. The inset is the variance of the difference between these two quantities in logarithmic scales normalized by the Kolmogorov acceleration and comparison with the St and $St^{1/2}$ power laws.

In contrast, for a bubble ($\beta = 3$), according to (3.4), the normalized acceleration variance increases as $\langle a_b^2 \rangle / a_\eta^2 - 1 \sim St^2$ and saturates to β^2 for $St \gg 1$. Note, however, that the limit $St \gg 1$ does not make sense, since for a bubble it implies $d_b^2/\eta^2 \gg 1$ which disagrees with the pointwise model. From the experimental results of Prakash *et al.* (2012) and the numerical simulations with a Faxén correction term (Calzavarini *et al.* 2009), also plotted in figure 1 for completeness, it appears that the finite size effect becomes important from $St \approx 2$ or $d_b/\eta \approx 7$, and leads to a decrease of the acceleration variance with a further increase of the bubble diameter (or Stokes number).

To analyse the substitution of the fluid velocity material derivative at the bubble position, $\mathrm{D}\boldsymbol{u}_f/\mathrm{D}t$, by its Lagrangian derivative along the bubble trajectory, $\mathrm{d}\boldsymbol{u}_f/\mathrm{d}t$, implied in (3.1), we remark that the material derivative can be written as $\mathrm{D}\boldsymbol{u}_f/\mathrm{D}t = \mathrm{d}\boldsymbol{u}_f/\mathrm{d}t + (\boldsymbol{u}_f - \boldsymbol{u}_p) \cdot \nabla \boldsymbol{u}_f$. We estimate that the order of magnitude of the last term is $O((\boldsymbol{u}_f - \boldsymbol{u}_p) \cdot \nabla \boldsymbol{u}_f) = \langle \boldsymbol{F}_d^2 \rangle^{1/2} St$, $\boldsymbol{F}_d$ being the drag force. Therefore, based on the previously disused scaling of the inertial particle acceleration we expect that this term grows linearly with St for $St \ll 1$ and as $St^{1/2}$ for $1 \ll St \ll \sqrt{Re_0}$ (see also the relation for the variance of the drag force proposed latter in (3.6)). Note that to obtain the previous estimation we have assumed that velocity gradients are of order $1/\tau_\eta$ and thus we neglected intermittency effects which probably leads to an underestimation at large Reynolds numbers. As shown in the inset of figure 2(*b*) the proposed scaling for the difference appears to be consistent with the DNS. To analyse further the error due to the simplification of the fluid inertia term we have computed, from the DNS, the variances of $\mathrm{D}\boldsymbol{u}_f/\mathrm{D}t$ and $\mathrm{d}\boldsymbol{u}_f/\mathrm{d}t$. It is seen in figure 2(*b*) that for $St < 0.2$ the variance of the time derivative of the fluid velocity along the bubble trajectory remains sizable to the variance of the fluid acceleration at the

bubble position (around 10 % of difference) while, for $St = 1$, it is larger by a factor of roughly 3. Moreover, the normalized p.d.f. of these two quantities (not shown) remains quite similar even for the largest Stokes number considered here. We can then conclude that our approximation is reasonable for $St < 1$ and could lead to an overestimation of the fluid inertia term for larger St. Nevertheless, the range of validity of the substitution and of the pointwise bubble approximation are seen to coincide.

The expression (3.5) does not include any intermittency effects and Reynolds number dependence (Yeung *et al.* 2006). The intermittent behaviour of the dissipation rate which is accounted for by the stochastic models discussed in §4 is associated with large fluctuations of the acceleration (Kolmogorov 1962; Castaing, Gagne & Hopfinger 1990; Lukassen & Wilczek 2017). This is seen in figure 3 presenting the bubble acceleration p.d.f. obtained from the DNS. It is observed that the bubble acceleration p.d.f. clearly presents a non-Gaussian behaviour with stretched tails indicating the occurrence of very intense acceleration events as pointed by Volk *et al.* (2008*a*), Prakash *et al.* (2012) and Loisy & Naso (2017). For intermediate Stokes number ($St \approx 0.5$) the bubble acceleration p.d.f. appears even more stretched than the p.d.f. of fluid tracer acceleration. While a further increase of St gives again a p.d.f. very similar to the p.d.f. of fluid tracer acceleration. Correspondingly, figure 3(*b*) shows that the bubble acceleration flatness ($Fl_a = \langle(\boldsymbol{a}_b - \langle\boldsymbol{a}_b\rangle)^4\rangle / \langle(\boldsymbol{a}_b - \langle\boldsymbol{a}_b\rangle)^2\rangle^2$) presents a maximum for a Stokes number around 0.2. Note that a peak was also observed in Calzavarini *et al.* (2009) but with a smaller maximum value and for a larger value of St. The difference is attributed to the smaller value of β and Re_λ ($\beta = 2.5$ and $Re_\lambda = 75$) used in Calzavarini *et al.* (2009). In this figure we also compare the flatness of fluid acceleration at the bubble position (or equivalently the flatness of the inertia force). It is observed that its value increases with St, but remains much smaller than the bubble acceleration flatness for intermediate Stokes numbers. As discussed below, the non-monotonic evolution of the bubble acceleration flatness is attributed to specific geometrical arrangements of the hydrodynamic forces applied to the bubble, rather than to a preferential concentration of bubbles in special regions of the flow (Calzavarini *et al.* 2008; Tagawa *et al.* 2012). Given the very large values taken by the flatness, this statistic might not be well converged, nevertheless there is no doubt that the flatness of the acceleration of the bubbles is much greater than that of the acceleration of the fluid at the bubble position.

From the relation (3.1) it is as well possible to obtain an estimate for the variance of the two terms on the right-hand side of (2.1), the drag force $\boldsymbol{F}_D = -(1/\tau_b)(\boldsymbol{u}_b(t) - \boldsymbol{u}_f(\boldsymbol{x} = \boldsymbol{x}_b(t), t))$, and the fluid inertia effect $\boldsymbol{F}_I = \beta(\mathrm{D}\boldsymbol{u}_f/\mathrm{D}t)(\boldsymbol{x} = \boldsymbol{x}_b(t), t)$,

$$
\begin{aligned}
\langle \boldsymbol{F}_D^2 \rangle &\approx \int_0^{k_1\omega_\eta} E_f(\omega)\frac{\omega^2(1-\beta)^2}{1+\omega^2\tau_b^2}\,\mathrm{d}\omega \\
&\approx c_0 a_\eta^2 \frac{(1-\beta)^2}{1-St_0^2}\left(\frac{\tan^{-1}(c_1 St)}{c_1 St} - \frac{\tan^{-1}(c_1 Re_0^{1/2})}{c_1 Re_0^{1/2}}\right)
\end{aligned}
\tag{3.6}
$$

$$
\begin{aligned}
\langle \boldsymbol{F}_I^2 \rangle &\approx \int_0^{k_1\omega_\eta} E_f(\omega)\omega^2\beta^2\,\mathrm{d}\omega \\
&\approx c_0 a_\eta^2 \beta^2 \left(1 - \frac{\tan^{-1}(c_1 Re_0^{1/2})}{c_1 Re_0^{1/2}}\right).
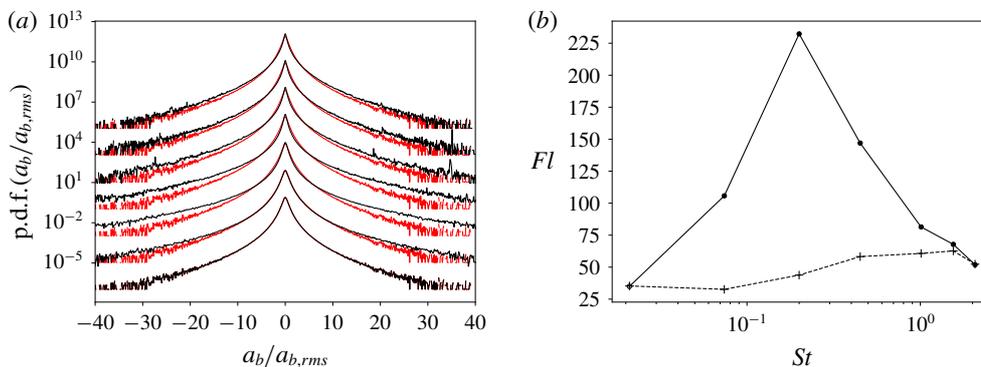\end{aligned}
\tag{3.7}
$$

FIGURE 3. (Colour online) (a) The p.d.f.s of the bubble acceleration normalized by its root-mean-square value in black for $St = 0.02$, 0.074, 0.20, 0.45, 1.01, 1.55 and 2.07 (shifted upward by two decades from each other for clarity, respectively) and comparison with the p.d.f.s of the acceleration of fluid tracers in red. (b) Flatness of the bubble acceleration ($\bullet$) and of the fluid acceleration at the bubble position ($+$) against St from our DNS.

These relations are plotted in figure 4(a) and are compared with the variance of the forces obtained from our DNS. Similar to the estimation of the acceleration variance expressions (3.6) and (3.7) are seen to provide a good estimation of the variances of $\boldsymbol{F}_D$ and $\boldsymbol{F}_I$ although the drag force is overestimated and the inertia force given by (3.7) is independent of the Stokes number which disagrees with the observation of figure 2(b). It is seen that for small Stokes numbers the variance of the two forces are commensurate, although the fluid inertia effect is dominant. Precisely, for $St \rightarrow 0$ the variance of the drag force is $(2/3)^2$ of that of the inertia term. It is also observed that the sum of the variance of the two forces is much larger than the variance of the bubble acceleration indicating a significant correlation between the two terms. As expected, when the Stokes number is increased, the drag force becomes negligible and the bubble acceleration is essentially given by the fluid inertia term.

Figure 4(b) presents the p.d.f. of both drag and fluid inertia forces for the various Stokes numbers. It is observed that for vanishingly small Stokes numbers ($St = 0.02$) the p.d.f.s of the two forces are essentially identical, and present both developed tails. The increase of the Stokes number results in a significant reduction of the tails of the drag force's p.d.f. whereas the p.d.f. of the inertia force presents very little variation (see also its flatness in figure 3). It is also worth mentioning that the p.d.f. of both forces remain symmetrical for all Stokes number indicating that the average and the skewness values of the two forces are zero. Because the bubbles sample regions of the flow in which the fluid acceleration variance is slightly below its overall value (see figure 2) and that the p.d.f. of the fluid acceleration at the bubble position is nearly invariant with the Stokes number, we conclude that the maximum of the bubble acceleration flatness is not caused by preferential concentration effects but is rather due to the alignment of the hydrodynamic forces on the bubble.

In figure 5(a), we plot the evolution of the correlation between $\boldsymbol{F}_D$ and $\boldsymbol{F}_I$ with the Stokes number obtained from the DNS. It is seen that for small St the two forces are completely anticorrelated, while they progressively decorrelate as St increases. Indeed requiring that for $St = 0$ the acceleration is equal to the acceleration of a fluid tracer, we obtain from (2.1) that $\boldsymbol{F}_D = (1 - \beta)/\beta \boldsymbol{F}_I$, that gives an anti-alignment for $\beta > 1$.
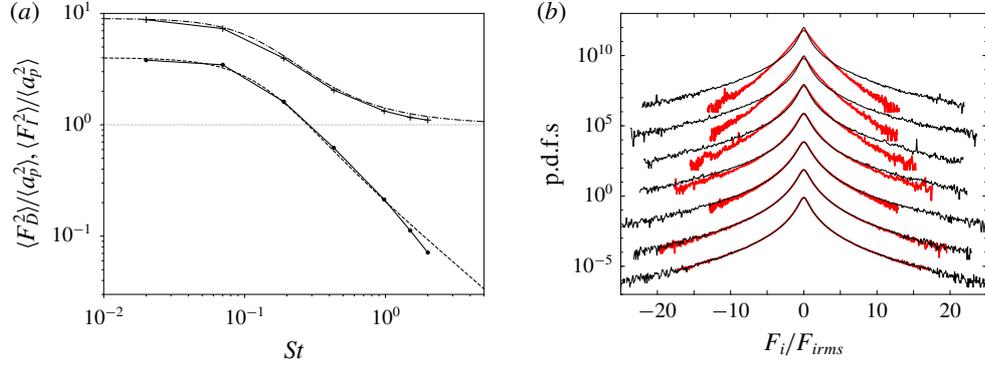
FIGURE 4. (Colour online) (*a*) Evolution with the Stokes number of the variance of the drag force (circle) and inertia force (crosses) relative to the bubble acceleration variance according to our DNS and comparison with (3.6) and (3.7) normalized by (3.4) with $c_1 = 2.8$ and $Re_0^{1/2} = 16$ in dashed and dot-dashed lines, respectively. (*b*) The p.d.f. of the fluid inertia forces (black) and of the drag force (red) normalized by their root-mean-square value for $St = 0.02, 0.074, 0.20, 0.45, 1.01, 1.55$ and 2.07 (shifted upward by one decade from each other for clarity, respectively).

Further, the correlation can also be readily estimated for larger Stokes numbers from (3.6), (3.7) and (3.4) as follows:

$$\langle \boldsymbol{F}_D \boldsymbol{\cdot} \boldsymbol{F}_I \rangle \approx c_0 a_\eta^2 \frac{\beta(1-\beta)}{1-St_0^2} \left(\frac{\tan^{-1}(c_1 St)}{c_1 St} - \frac{\tan^{-1}(c_1 Re_0^{1/2})}{c_1 Re_0^{1/2}} \right). \tag{3.8}$$

Figure 5(*a*) shows that the relation (3.8) is in good agreement with the DNS results. Further, if the persistence of the temporal autocorrelation of the norms of the two forces is much longer than for their orientation, then the correlation between the two forces could be approximated by their relative orientation,

$$\langle \boldsymbol{F}_D \boldsymbol{\cdot} \boldsymbol{F}_I \rangle \approx \langle \cos\theta \rangle (\langle \boldsymbol{F}_D^2 \rangle \langle \boldsymbol{F}_I^2 \rangle)^{1/2}, \tag{3.9}$$

where θ is defined as $\cos\theta = \boldsymbol{F}_D \boldsymbol{\cdot} \boldsymbol{F}_I / |\boldsymbol{F}_D||\boldsymbol{F}_I| = \boldsymbol{e}_I \boldsymbol{\cdot} \boldsymbol{e}_D$, with $\boldsymbol{e}_I$ and $\boldsymbol{e}_D$ the orientation vectors of the inertia term and of the drag force, respectively. This is confirmed in figure 5(*a*) that indeed $\langle \cos\theta \rangle$ remains quite close to $\langle \boldsymbol{F}_D \boldsymbol{\cdot} \boldsymbol{F}_I \rangle (\langle \boldsymbol{F}_D^2 \rangle \langle \boldsymbol{F}_I^2 \rangle)^{-1/2}$. Figure 5(*b*) reports the evolution with the Stokes number of the p.d.f. of $\cos\theta$. For small Stokes numbers, the two forces appear to be essentially anti-aligned as the p.d.f. presents a sharp peak around -1 consistent with its averaged value. When the Stokes number is increased, the distribution of $\cos\theta$ becomes flatter, indicating that the relative orientation of the two forces becomes progressively statistically isotropic. Note that according to (3.8) we should expect a positive correlation between the two forces for $\beta < 1$ and small St.

In figure 6(*a*), we present the evolution of the Lagrangian autocorrelation of the bubble acceleration for the various Stokes numbers. It is observed that an increase of the Stokes number produces a faster decorrelation, as already reported by Volk *et al.* (2008*b*), although for $0 < St < 2$ it is seen that the correlation time remains of order τ_η. It is worth mentioning that this behaviour departs significantly from the evolution of inertial particles which present larger correlation time with increasing St (Gorokhovski
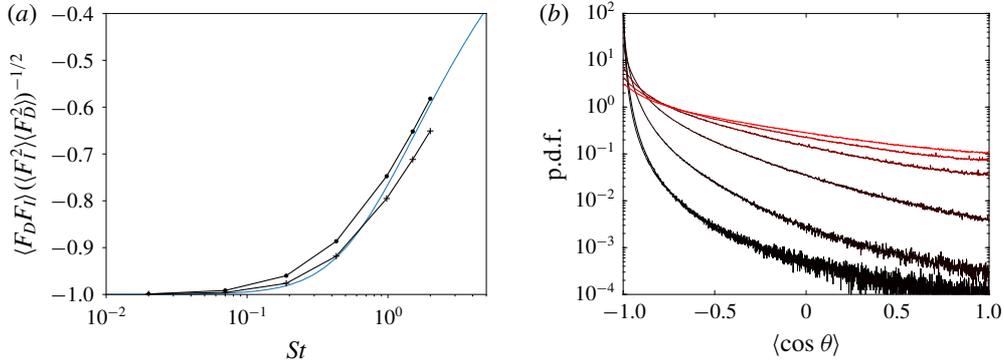
FIGURE 5. (Colour online) (a) Evolution with St of the coefficient of correlation between the drag and inertia forces (dots) and of $\langle\cos\theta\rangle$ (θ being the relative orientation of the forces) (crosses) from the DNS and comparison with relation (3.8) normalized by (3.6) and (3.7) with $c_1 = 2.8$ and $Re_0^{1/2} = 16$ in blue lines. (b) The p.d.f.s of the cosine of the angle θ between the two forces, for $St = 0.02$, 0.074, 0.20, 0.45, 1.01, 1.55 and 2.07 (from black to red, respectively).

& Zamansky 2018). To further analyse this point, we also present, in figure 6(a), the autocorrelation along the bubble trajectory of the two forces acting on the bubble. It is observed that for vanishingly small Stokes number, the two forces present exactly the same evolution of their Lagrangian correlation, because of the almost instantaneous response of the drag force to the inertia force. With increasing the Stokes number, one sees a clear difference in the autocorrelation of the drag force and of the inertia forces. Increasing the Stokes number gives a longer persistence time for the drag forces which can be directly attributed to the increase of τ_b. On the other hand, the faster decorrelation of the inertia force is explained by the deviation of the bubble trajectories from the fluid tracer trajectories.

The response of the drag force to the inertia term is analysed in figure 6(b) which presents the plot of the cross correlation of the orientation of the two forces along the bubble trajectory. The cross-correlation is defined as $\rho_{e_D,e_I} = \langle -e_I(t) \cdot e_D(t + \tau)\rangle/(\langle e_I^2\rangle\langle e_D^2\rangle)^{1/2}$. This figure confirms that the orientation of the drag forces responds to the inertia term. The temporal lag between the two forces can be estimated from the time shift of the peak, $\max_\tau(\rho_{e_D,e_I}(\tau)) = \rho_{e_D,e_I}(\tau_{lag})$. In the inset of figure 6(a), we present the evolution of τ_{lag} with St. It is seen that τ_{lag} presents a linear evolution for small τ_b. Indeed for vanishingly small Stokes number, the drag responds instantaneously. For larger Stokes number, the growth rate of τ_{lag} reduces. We observe that $\tau_{lag} \approx \tau_\eta(\beta - 1)^{-1} \tan^{-1}((\beta - 1)St)$ is a relatively good approximation of the lag of the drag force compared to the inertia effect. Clearly a further check of this speculative relation would require simulations for different values of β. We remark that one could estimate the autocorrelation of the bubble acceleration or hydrodynamic forces as well as the cross-correlation presented in figure 6 from the spectral response model of (3.1). However, this would require a more precise estimation of the Lagrangian fluid velocity spectra at high frequency than the relation (3.3), as the decorrelation is controlled by the dissipative range of the spectra which depend on St as seen in figure 2.

The anti-alignment of the forces at small Stokes can be explained as follows. For vanishingly small Stokes number, the relaxation time τ_b of the bubble velocity to the
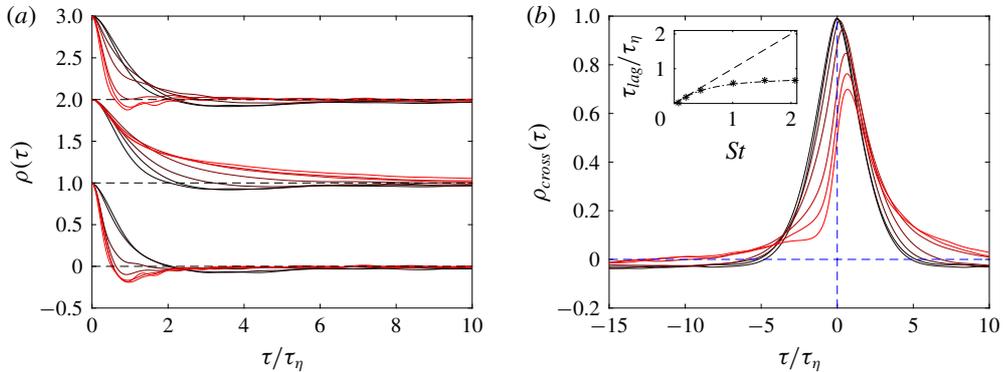
FIGURE 6. (Colour online) (a) Autocorrelation coefficient of the bubble acceleration, drag force and fluid inertia terms (shifted upward by one unit from each other, respectively, for clarity) from our DNS. (b) Cross-correlation between the drag force and the fluid inertia term as given by our DNS. The inset is the evolution of the time lag (defined as the time of the peak of cross-correlation) with St, and comparison with the $\tau_{lag}/\tau_\eta = St$ and $\tau_{lag}/\tau_\eta = (\beta - 1)^{-1} \tan^{-1}((\beta - 1)St)$. For both figures $St = 0.02$, 0.074, 0.20, 0.45, 1.01, 1.55 and 2.07 (from black to red, respectively).

local fluid velocity is much smaller than the persistence time of the fluid inertia term, which is of order τ_η (Pope 1990; Mordant *et al.* 2004). Therefore, the drag force will very quickly respond, leading it to be statistically opposed to the fluid inertia term. On the other hand, for $St \gg 1$ we should expect that the orientation of the two forces becomes independent because the relaxation time of the particle becomes much larger than τ_η. In the meantime, we have observed that the amplitude of the drag forces becomes negligible as the Stokes number is increased. This conjunction of the evolution of the relative orientation and magnitude of the two forces, leads to the increases of the bubble acceleration flatness, observed in figure 3 for St around 0.5. For these Stokes numbers, the amplitude of the drag forces remains significant while its orientation already presents a wide distribution, leading to the strong intermittency of the acceleration, when the two forces, of similar magnitude, are anti-aligned the acceleration will be close to zero whereas in case of an alignment of the forces intense acceleration will result.

We have proposed above a relation between the bubble acceleration variance and the average dissipation rate. However, in line with the Kolmogorov theory, the instantaneous acceleration depends *a priori* on the local energy dissipation rate ε. To discuss this point we present in figure 7 statistics of the bubble acceleration conditioned on the local value of the dissipation rate. This is also motivated to provide supports for a stochastic modelling of the bubble acceleration that accounts for the large fluid fluctuations in small-scale motions, as discuss in the following section. We consider in figure 7(a) the variance of the bubble acceleration conditioned on the local dissipation rate. We first observe that for ε larger than its average value, $\langle a_b^2 | \varepsilon \rangle$ appears to be independent of the Stokes number, and increases as $\varepsilon^{3/2}$, while it presents little dependence on both ε and St for small value of ε,

$$\langle \boldsymbol{a}_b^2 | \varepsilon \rangle \approx \langle \boldsymbol{a}_b^2 \rangle \left(\frac{\varepsilon}{\langle \varepsilon \rangle} \right)^{3/2}; \quad \varepsilon > \langle \varepsilon \rangle. \tag{3.10}$$
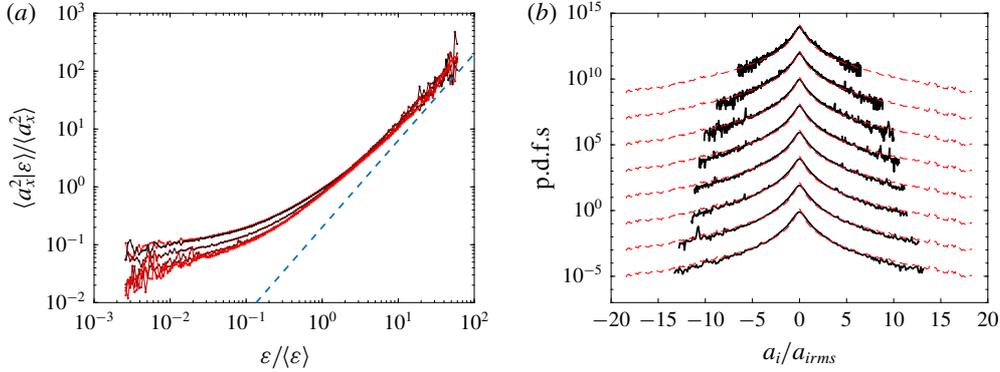
FIGURE 7. (Colour online) (*a*) Variance of the bubble acceleration conditioned on the local value of the dissipation rate ε for the various Stokes number $St = 0.02, 0.074, 0.20, 0.45, 1.01, 1.55$ and 2.07 (from black to red, respectively) normalized by unconditional bubble acceleration variance, and comparison with the relation $\langle a_b^2 | \varepsilon \rangle / \langle a_b^2 \rangle = (\varepsilon / \langle \varepsilon \rangle)^{3/2}$ with a dashed line. (*b*) The p.d.f.s of acceleration conditioned on the dissipation rate for $St = 1$. Eight values of ε are reported, $\varepsilon / \langle \varepsilon \rangle = 0.17, 0.28, 0.46, 0.77, 1.3, 2.1, 3.5$ and 5.8 (shifted upward by two decades from each other, respectively) and comparison with unconditioned bubble acceleration p.d.f. with dashed lines.

This behaviour is similar to previous observations for fluid tracers from Yeung *et al.* (2006). The invariance with St observed for the micro-bubbles is therefore attributed to dominance of the fluid inertia term. It was reported by Yeung *et al.* (2006) that the exponent of the power law for the conditional acceleration is reduced for low values of Reynolds numbers. Also Yeung *et al.* (2006) showed that the value at which the acceleration variance converge for $\varepsilon \rightarrow 0$ decreases with Reynolds number, indicating that the acceleration in the weakly dissipative regions is primarily influenced by the large-scale sweeping. In figure 7(*b*) the conditional p.d.f. normalized by its standard deviation is shown to be approximately self-similar with ε. The conditional p.d.f.s present slightly less developed tails than the unconditional p.d.f., similarly to the observation of Yeung *et al.* (2006) for fluid particles. Note that in figure 7(*b*), the conditional p.d.f.s are shown for $St = 1$ but a similar conclusion holds for the other Stokes number studied here.

4. Stochastic modelling of the dynamics of micro-bubbles

Following the proposition of Gorokhovski & Zamansky (2018) (see also Sabel'nikov *et al.* 2007, 2011; Zamansky *et al.* 2013), the instantaneous acceleration of each bubble is decomposed into filtered and stochastic parts. The first term corresponds to the contribution to the sweep imposed by the large (resolved) scales of the flow, and the second term accounts for the unresolved fluctuations of the carrier phase

$$\boldsymbol{a}_b = \bar{\boldsymbol{a}}_b + \boldsymbol{a}^*. \tag{4.1}$$

The residual contribution $\boldsymbol{a}^*$ is determined by the drag forces and the fluid inertia effect (added mass and Tchen force), $\boldsymbol{a}^* = \boldsymbol{F}_D^* + \boldsymbol{F}_I^*$, which are both considered as random processes. The stochastic forces are both decomposed into a norm and an orientation process, $\boldsymbol{F}_D^* = |\boldsymbol{F}_D^*| \boldsymbol{e}_D^*$ and $\boldsymbol{F}_I^* = |\boldsymbol{F}_I^*| \boldsymbol{e}_I^*$. These decompositions are supported

by the separation of time scale of the evolution of the autocorrelation for the norm and the orientation, suggesting that the norm and orientation of each force can be treated as independent processes, similarly to Pope (1990), Mordant *et al.* (2004) and Sabel'nikov *et al.* (2011). However, as mentioned previously, the two forces present significant correlation (both for their norm and their orientation) and could not be considered as independent.

First, in line with the refined Kolmogorov assumption, the main source of randomness in the instantaneous norms of the forces is attributed to the local energy dissipation rate. Then by analogy with relation (3.10), we propose the following:

$$|\boldsymbol{F}_D^*| \approx \langle \boldsymbol{F}_D^{*2} | \varepsilon_* \rangle^{1/2} \approx \langle \boldsymbol{F}_D^{*2} \rangle^{1/2} \left(\frac{\varepsilon_*}{\langle \varepsilon \rangle} \right)^{3/4}, \tag{4.2}$$

$$|\boldsymbol{F}_I^*| \approx \langle \boldsymbol{F}_I^{*2} | \varepsilon_* \rangle^{1/2} \approx \langle \boldsymbol{F}_I^{*2} \rangle^{1/2} \left(\frac{\varepsilon_*}{\langle \varepsilon \rangle} \right)^{3/4}. \tag{4.3}$$

In these relations, ε_* is obtained from a stochastic process mimicking the evolution of the dissipation rate along the bubble trajectory. Since it is observed that the norm of the two forces are strongly correlated, ε_* is the same stochastic variable in both relations (4.2) and (4.3). It was indeed observed from the DNS that the norms of the two forces remain strongly correlated for all the Stokes numbers considered here, consistent with (3.9). In order to only consider the contribution from the unresolved fluctuations in the estimation of $\langle \boldsymbol{F}_D^{*2} \rangle$ and $\langle \boldsymbol{F}_I^{*2} \rangle$, the integrals (3.6) and (3.7) are truncated for $\omega < k_2 2\pi / \tau_\Delta$ with $\tau_\Delta = \Delta^2 / \nu_\Delta$ the time scale of the smallest eddies resolved by the mesh. And, as before, the integrals are also truncated for $\omega > k_1 \omega_\eta$ to ensure its convergence. Considering, for simplicity, the high Reynolds limit $Re_0 \gg 1$ and $Re_0 \gg St^2$, the estimation for the instantaneous norms are then given by

$$|\boldsymbol{F}_D^*| = c_0^{1/2} \varepsilon_*^{3/4} \nu^{-1/4} |1 - \beta| \left(\frac{\tan^{-1}(c_1 St)}{c_1 St} - \frac{\tan^{-1}(c_1 St Re_\Delta^{-1/2})}{c_1 St} \right)^{1/2}, \tag{4.4}$$

$$|\boldsymbol{F}_I^*| = c_0^{1/2} \varepsilon_*^{3/4} \nu^{-1/4} \beta (1 - Re_\Delta^{-1/2})^{1/2}, \tag{4.5}$$

where $Re_\Delta^{1/2} = (k_2/k_1)\tau_\Delta/\tau_\eta$ is a Reynolds number characteristic of the subgrid scale motion. This gives for $\boldsymbol{a}^*$,

$$\boldsymbol{a}^* = c_0^{1/2} \varepsilon_*^{3/4} \nu^{-1/4} \left[\frac{|1 - \beta|}{c_1 St} \left(\tan^{-1}(c_1 St) - \tan^{-1} \left(\frac{c_1 St}{Re_\Delta^{1/2}} \right) \right)^{1/2} \boldsymbol{e}_D^* + \beta (1 - Re_\Delta^{-1/2})^{1/2} \boldsymbol{e}_I^* \right]. \tag{4.6}$$

Note that when the mesh is refined ($\Delta \to \eta$), $Re_\Delta \to 1$ and the amplitude of the residual contributions vanish as expected, since for a sufficiently fine mesh the bubble dynamics should be captured by the resolved contribution. Concerning the evolution of the stochastic variable ε_*, assuming that it is given by a log-normal process that depends on the local value of ε_Δ computed from the coarse LES mesh, one obtains the following stochastic process for $\varepsilon_*^{3/4}$ similar to Pope & Chen (1990) (see also Gorokhovski & Zamansky 2018):

$$\frac{\mathrm{d}\varepsilon_*^{3/4}}{\varepsilon_*^{3/4}} = \frac{\mathrm{d}\varepsilon_\Delta^{3/4}}{\varepsilon_\Delta^{3/4}} - \left(\ln \left(\frac{\varepsilon_*^{3/4}}{\varepsilon_\Delta^{3/4}} \right) - \frac{3}{16} \sigma^2 \right) \frac{\mathrm{d}t}{\tau_\Delta} + \sqrt{\frac{9}{8} \frac{\sigma^2}{\tau_\Delta}} \, \mathrm{d}W, \tag{4.7}$$

where dW is the increment of the Wiener process and $d\varepsilon_\Delta^{3/4}$ is the increment of $\varepsilon_\Delta^{3/4}$ along the bubble trajectory. This stochastic process ensures that $\langle \varepsilon_* \rangle = \langle \varepsilon_\Delta \rangle$ (see the details in Gorokhovski & Zamansky (2018)), and the parameter σ is given by $\sigma^2 = 0.36 \ln Re_\Delta^{1/2}$ materializing the depth of the cascade process (Kolmogorov 1962; Castaing 1996), with the value of the coefficient in front of the logarithm set in order to reproduce the Reynolds number dependence reported by Yeung *et al.* (2006). The time scale τ_Δ imposes the temporal correlation of ε_*. Note that more sophisticated multiplicative models have been proposed for ε_* (Pereira, Moriconi & Chevillard 2018); however, in the present paper we have used the simple log-normal process (4.7).

The orientation vectors $\boldsymbol{e}_D^*$ and $\boldsymbol{e}_I^*$ appearing in (4.6) are given by two joint stochastic random walks on the unit sphere

$$d\boldsymbol{e}_I^* = \gamma_I \boldsymbol{e}_I^* \times \boldsymbol{\alpha}_I \, dt + (\gamma_I - 1)\boldsymbol{e}_I^*, \tag{4.8}$$

$$d\boldsymbol{e}_D^* = \gamma_D \boldsymbol{e}_D^* \times \boldsymbol{\alpha}_D \, dt + (\gamma_D - 1)\boldsymbol{e}_D^*, \tag{4.9}$$

with $\boldsymbol{\alpha}_I$ and $\boldsymbol{\alpha}_D$ the angular velocities of the evolution of $\boldsymbol{e}_I^*$ and $\boldsymbol{e}_D^*$ on the sphere and where the factors $\gamma_I = (1 + \boldsymbol{\alpha}_I.\boldsymbol{\alpha}_I \, dt^2 - (\boldsymbol{\alpha}_I \cdot \boldsymbol{e}_I^*)^2 \, dt^2)^{-1/2}$ and $\gamma_D = (1 + \boldsymbol{\alpha}_D.\boldsymbol{\alpha}_D \, dt^2 - (\boldsymbol{\alpha}_D \cdot \boldsymbol{e}_D^*)^2 \, dt^2)^{-1/2}$ correspond to a projection ensuring that the norms of both $\boldsymbol{e}_I^*$ and $\boldsymbol{e}_D^*$ remain unity (Gorokhovski & Zamansky 2018). The coupling of these two random walks, through the evolution of their angular velocities, is intended to reproduce the anti-alignment between the two orientation vectors observed for small Stokes number, and their decorrelation when St is increased as well as the correlation of the orientation with the coarse-grained (resolved) fluid acceleration. Moreover the temporal evolution of the random walks provides a temporal autocorrelation for the two orientations. The evolution of $\boldsymbol{\alpha}_I$ and $\boldsymbol{\alpha}_D$ is given by the following Ornstein–Uhlenbeck process presenting restoring terms, damping terms and diffusion terms:

$$d\boldsymbol{\alpha}_I = -\boldsymbol{e}_I^* \times \frac{D_t \overline{\boldsymbol{u}}_f}{\Delta} \, dt - \boldsymbol{\alpha}_I \frac{dt}{\tau_I} + \sqrt{\frac{\sigma_I^2}{\tau_I}} \, d\boldsymbol{W}_I, \tag{4.10}$$

$$d\boldsymbol{\alpha}_D = -\boldsymbol{e}_D^* \times \boldsymbol{e}_I^* \frac{dt}{\tau_r^2} - \boldsymbol{\alpha}_D \frac{dt}{\tau_D} + \sqrt{\frac{\sigma_D^2}{\tau_D}} \, d\boldsymbol{W}_D, \tag{4.11}$$

with $d\boldsymbol{W}_I$ and $d\boldsymbol{W}_D$ the increments of two independent three-dimensional Wiener processes. The diffusion terms provide a return to isotropy of both orientations as the randomness of the angular velocities lead $\boldsymbol{e}_D^*$ and $\boldsymbol{e}_I^*$ to visit every point of the sphere. The temporal autocorrelation of both $\boldsymbol{e}_D^*$ and $\boldsymbol{e}_I^*$ is then related to the diffusion coefficient of the angular velocity. On the other hand, the restoring terms tend to align $\boldsymbol{e}_D^*$ and $\boldsymbol{e}_I^*$ with some equilibrium orientation.

For small values of τ_Δ/τ_η, we expect to have an alignment of the fluid acceleration model onto the coarse-grained fluid acceleration, while for τ_Δ/τ_η large, the alignment with the resolved acceleration should be weak, in agreement with the local isotropy assumption (Kolmogorov 1941). Therefore, in our model, we propose to have an alignment of the orientations of the subgrid contribution of the fluid acceleration to the coarse-grained fluid acceleration orientation $\overline{D_t \boldsymbol{u}_f}/|\overline{D_t \boldsymbol{u}_f}|$. The alignment between them is controlled by the restoring term in (4.10) and the time scale $(|\overline{D_t \boldsymbol{u}_f}|/\Delta)^{-1/2} \approx \tau_\Delta$.

The restoring term in (4.11) will tend to align $\boldsymbol{e}_D^*$ on $-\boldsymbol{e}_I^*$ in agreement with the observations of § 3. The rate of alignment is given by the parameters τ_r. Since the
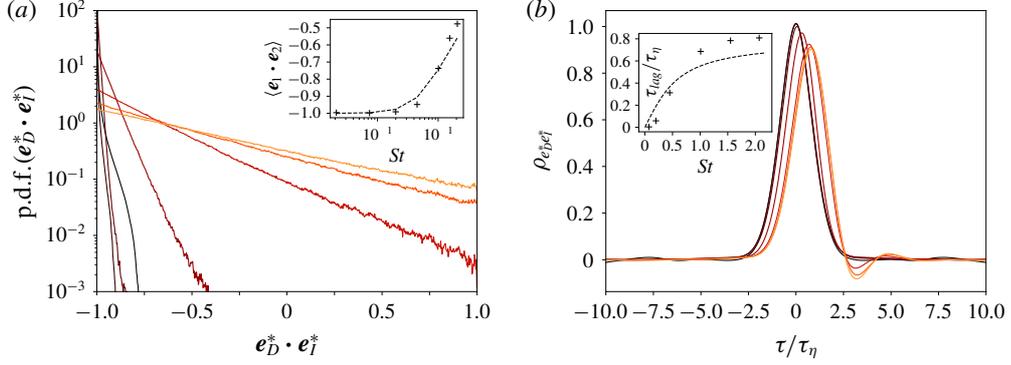
FIGURE 8. (Colour online) (*a*) The p.d.f.s of $e_I^* \cdot e_D^*$ for $St = 0.02$, 0.074, 0.20, 0.45, 1.01, 1.55 and 2.07 (from black to red, respectively) as obtained from model (4.8)–(4.11). The inset is the evolution of $\langle e_D^* \cdot e_I^* \rangle$ with St as given by the stochastic model, and comparison with the relation (3.8). (*b*) Cross-correlation between e_D^* and e_I^* obtained from the model (4.8)–(4.11). The inset is the evolution of the time lag between e_D^* and e_I^* against St, and comparison with $\tau_\eta(\beta - 1)^{-1} \tan^{-1}((\beta - 1)St)$.

latter should coincide with the time lag observed in the cross-correlation between the orientation of the two forces (see figure 6), we set $\tau_r = \tau_\eta(\beta - 1)^{-1} \tan^{-1}((\beta - 1)St)$. This ensures that the drag force correlation time increases with the Stokes number as observed in figure 6.

The other parameters in (4.10) are set to $\tau_I = \tau_\eta$ and $\sigma_I^2 = \tau_\eta^{-2}$ which ensure that the temporal autocorrelation of the fluid acceleration orientation is of the order of τ_η in agreement with the experimental findings of Mordant *et al.* (2004) and our DNS (see figure 6). In (4.11) the parameters are set to $\tau_D = (\tau_b + \tau_\eta)/4$ and $\sigma_D^2 = (\tau_b + \tau_\eta)^{-2}/2$ consistent with Gorokhovski & Zamansky (2018).

Figure 8(*a*) presents the evolution of the p.d.f. of the relative orientation between the two forces $\cos \theta^* = e_D^* \cdot e_I^*$, obtained from numerical integration of the stochastic orientation model (4.8)–(4.11) (and setting $D_t \overline{u}_f = 0$ in (4.8)). We clearly observe that at small Stokes number the model predicts an anti-alignment between the two orientation vectors while their relative orientation becomes more isotropic when the Stokes number increases. This behaviour is in agreement with the statistics computed from the DNS (see figure 5*b*), although the p.d.f. from the DNS present a more stretched tail. It is also confirmed in the inset of figure 8(*a*) that the proposed stochastic model gives the correct evolution of the average relative orientation with the Stokes number, since as in the DNS case $\langle \cos \theta^* \rangle$ follow the relation (3.8). The cross-correlation between e_D^* and e_I^* is also presented in figure 8(*b*). The behaviour of the DNS observed in figure 6 can be qualitatively reproduced by the stochastic model with an increase of the time lag with the Stokes number.

The resolved contribution in (4.1) is obtained from a spatially and temporarily averaged version of (2.1). The spatial average arises from substituting the actual velocity field u_f to the coarse-grained velocity field $\overline{u}_f$ in this equation. In addition, a temporal filter is also explicitly applied to prevent the term $\overline{a}$ developing high frequencies that would correlate with the residual term. Removing the frequencies above $1/\tau_\Delta$ results in the following expression for $\overline{a}$ (see also Gorokhovski & Zamansky 2018):

$$\overline{a} = -\frac{u_b - \overline{u}_f}{\max(\tau_b, \tau_\Delta)} + \beta \frac{D\overline{u}_f}{Dt}, \tag{4.12}$$

where $D_t \overline{\boldsymbol{u}}_f = \partial_t \overline{\boldsymbol{u}}_f + \overline{\boldsymbol{u}}_f \cdot \nabla \overline{\boldsymbol{u}}_f$ is the fluid total acceleration computed from the coarse mesh. Note that one does not have to necessarily consider the coupling with the LES to use the proposed model. Indeed, by considering the limit $\Delta \to L$, L being the integral length scale, the term $\overline{\boldsymbol{a}}$ vanishes and (4.1) becomes $\boldsymbol{a}_b = \boldsymbol{a}^*$. As well, in this limit one can replace $\varepsilon_\Delta(t)$ in (4.7) by the constant value $\langle \varepsilon \rangle$. For example, one can estimate the Reynolds number dependence for the intermittency correction in (3.5) from the moments of a log-normal variable, to be $\langle \boldsymbol{a}_b^2 \rangle / a_\eta^2 \propto \exp(3/8\,\sigma^2) = Re_\lambda^{0.135}$, as proposed by Yeung *et al.* (2006).

In order to assess the approach (4.1) as well as the stochastic model proposed in (4.6)–(4.11), we present a comparison of the statistics of the bubble dynamics obtained from the DNS, the standard LES (without modelling of the residual bubble acceleration i.e. setting $\boldsymbol{a}^* = 0$ in (4.1)), and the LES with the proposed model. All the comparisons are made for $Re_\lambda \approx 200$ and three resolutions are used for the LES (32^3, 48^3 and 64^3) while the resolution of the DNS is 1024^3. The details of the LES are given in § 2.

We first present in figure 9(*a*) the evolution of the bubble acceleration variance with the Stokes number. We observe that the standard LES largely underestimates the bubble acceleration variance compared to the DNS. As expected the discrepancy increases as the mesh resolution is made coarser. This points out that the residual term in (4.1) is dominant. In contrast, the LES supplemented by the stochastic modelling is in very good agreement with the DNS. Moreover, with the stochastic model, the LES presents a very small dependence on the grid resolution. This confirms that the effects of the unresolved small scales of the flow are correctly accounted for by the model.

Figure 9(*b*) presents the p.d.f. of the bubble acceleration for the various Stokes numbers. It is seen that the standard LES predicts p.d.f.s that depart significantly from the DNS and remain much closer to the Gaussian distribution. On the other hand, the p.d.f.s from the LES with the stochastic model overlap very well with the p.d.f.s of the DNS over the whole range of Stokes numbers considered here. This shows that the intermittent behaviour of the bubble acceleration can be reproduced with the proposed stochastic model.

We consider in figure 10 the autocorrelation of the acceleration component. As illustrated for $St = 1$, the decorrelation of the acceleration is much slower from the LES than from the DNS. This is expected since the decorrelation of the acceleration component is attributed to the small-scale motions of the flow which are discarded in the LES. For the LES supplemented with the model the evolution of the correlation coefficient presents qualitative agreement with the DNS. This behaviour is confirmed in the inset of figure 10 which presents the correlation time, defined as the zero crossing time, against the Stokes number. It is observed that the correlation times obtained from the DNS and from the LES with the model both remain of the order of τ_η, whereas the standard LES predicts a much larger correlation time. We observe that the orientation model plays an essential role in obtaining an accurate estimation of the decorrelation time, and it is likely that an improvement of the model given by (4.8)–(4.11) could reduce the small discrepancies seen between the LES using the model and the DNS.

To evaluate the capability of the stochastic approach to accurately reproduce the time structure of the bubble velocity, we report in figure 11 the statistic of the velocity increments along the bubble trajectory. For that, we consider the structure function for a component of the bubble velocity $S_q(\tau) = \langle (u_{b,x}(t + \tau) - u_{b,x}(t))^q \rangle$. In figure 11(*a*) we present the evolution of the variance of the velocity increments, S_2,
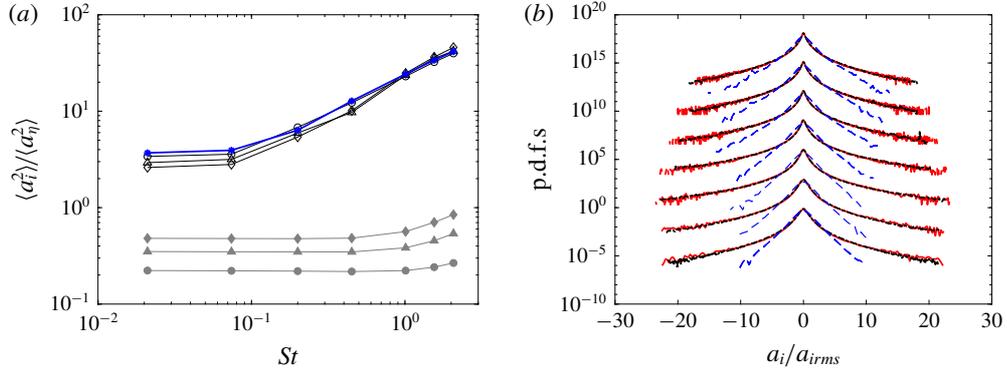
FIGURE 9. (Colour online) (*a*) Bubble acceleration variance normalized by the Kolmogorov acceleration (a_η^2) versus Stokes number in logarithm scale. Open symbols are LES with the proposed model; filled symbols are LES without model; for the three meshes we have 32^3 (circles), 48^3 (triangles) and 64^3 (diamonds). Comparison with our DNS blue stars. (*b*) The p.d.f. of the bubble acceleration normalized by its variance for $St = 0.02$, 0.074, 0.20, 0.45, 1.01, 1.55 and 2.07 (shifted upward by one decade each other, respectively). The DNS is a dashed black line, LES with the proposed model for 64^3 is a solid red line and LES without model for 64^3 is a blue dashed line.
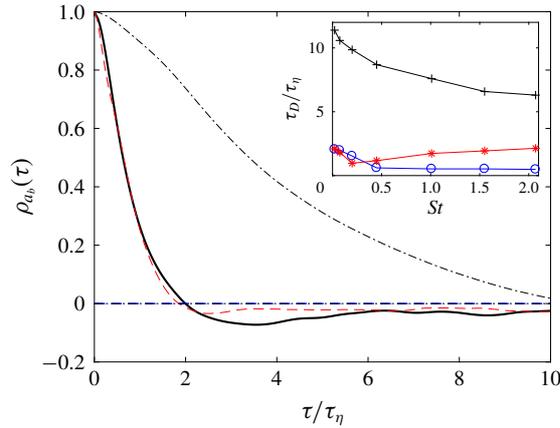

FIGURE 10. (Colour online) Autocorrelation of the bubble acceleration for $St = 0.07$. The DNS is a solid black line, LES with model for 64^3 is a dashed red line and LES without model for 64^3 is a dot-dashed black line. The inset is the evolution of the corresponding integral time scale normalized by the Kolmogorov time with the Stokes number. The DNS are circles, LES with the proposed model are stars, LES without model are crosses. The mesh size for the LES is 64^3.

with the time shift. The results from the LES with the proposed model follow very well those obtained from the DNS, whereas with the standard LES, the variance of the velocity increments is largely underestimated. Moreover, we observe that with the stochastic model the LES can reproduce the inertial range as observed from the DNS contrary to the standard LES. Figure 11(*b*) shows the evolution of the flatness of the bubble velocity increments, S_4/S_2^2. We see that with the standard LES the flatness
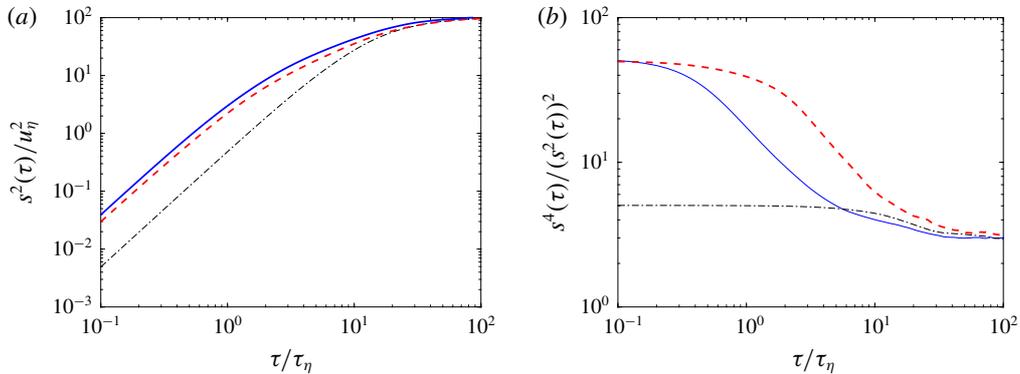
FIGURE 11. (Colour online) (*a*) Evolution of the second-order Lagrangian structure function with the time lag. (*b*) Evolution of the flatness of the Lagrangian velocity increments with the time lag. Comparison between the DNS (solid blue line), the Standard LES (black dot-dashed lines) and LES with the proposed model (dashed red lines). For both figures, for $St = 0.02$, the mesh size for the LES is 64^3.

remains close to its Gaussian value at all time shifts. In contrast, the LES with the proposed model gives an evolution of the flatness in agreement with the DNS, presenting a value close to 3 at large τ and a significant increase with a reduction of the time shift. One can then conclude that intermittency effects associated with the small scales of the velocity field can be captured by the LES supplemented by the proposed model. Note that in figure 11 we have presented the evolution of the structure function for $St = 1$, but the same behaviour is obtained for the other values of Stokes number considered here.

We present in figure 12, $\langle a_b^2 | \varepsilon_* \rangle$, the variance of the bubble acceleration conditioned on the value of the instantaneous value of the dissipation rate ε_* estimated from the stochastic model (4.7). It is observed that similar to the DNS results reported in the figure 7, the bubble acceleration from the LES with the model increases as $\varepsilon_*^{3/2}$ for large values of the dissipation rate, and is independent on ε_* for the small values of the latter. This behaviour shows that the acceleration of the bubbles in the weakly dissipative regions can be computed by the resolved contribution $\bar{a}_b$, indicating the influence of the large-scale sweeps, while the largest fluctuation of the acceleration are correctly estimated with the stochastic model.

5. Conclusion

In this paper, we study the statistics of the acceleration and forces of micro-bubbles ($\eta > d_b$) subject to the drag and fluid inertia forces in a homogenous and isotropic turbulent flow. For small Stokes numbers, the two forces are commensurate and are found to be preferentially anti-aligned, whereas for larger Stokes numbers the drag force becomes negligible and the bubble acceleration is essentially given by the fluid inertia forces resulting in a bubble acceleration variance larger than for fluid tracers. We propose an analytical model, depending on the Stokes number, Reynolds number and the density ratio, describing qualitatively these observations. The model based on the spectral response of the bubble to the fluid fluctuations (similar to the Tchen theory) assumes firstly the shape for the frequency spectra of the fluid velocity along the bubble position (with a ω^{-2} power law), and secondly that the material derivative
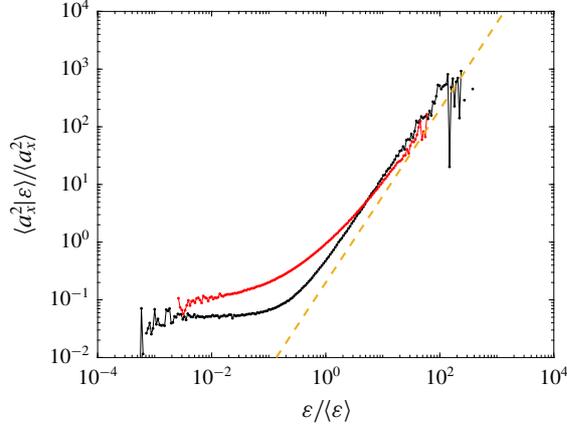
FIGURE 12. (Colour online) Variance of the total bubble acceleration $\boldsymbol{a}_b = \bar{\boldsymbol{a}}_b + \boldsymbol{a}_*$ conditioned on the stochastic value of the dissipation rate ε_* obtained from the LES with the stochastic model (black line) and comparison with the bubble acceleration variance conditioned on the local dissipation rate obtained from the DNS (red line), with $St = 0.02$ and a mesh size of 48^3 for the LES.

of the fluid velocity at the bubble position can be substituted by the time derivative along the bubble trajectories. These assumptions lead to fairly accurate estimations for small St, and some deviations are observed for $St \approx 1$ as the preferential concentration of bubbles is not accounted for. This effect could be taken into account in the model, by providing more precise, St dependent, estimation of the high frequency part of the Lagrangian fluid velocity spectra and of the fluid acceleration variance at the bubble position. It is further observed that the micro-bubble acceleration conditioned on the local dissipation rate presents a surprising invariance. For values of the local dissipation rate similar or larger than the average one, the conditional acceleration variance appears to be invariant with the Stokes number and increases with the dissipation rate, whereas the conditional p.d.f. are observed to be nearly invariant with the dissipation rate and the Stokes number when normalized by the conditional variance. Such invariance was not expected because of the very intense clustering of the bubbles reported by Calzavarini *et al.* (2008) around $St = 1$. Indeed, at small Stokes number the bubbles behave like fluid tracers, whereas for Stokes numbers of order 1 (for which one can neglect the drag force) the acceleration of a bubble is roughly $\beta = 3$ times that of a tracer at the same position. Nevertheless the near invariance of the conditional statistics implies that in the two cases the bubbles sample fluid regions in which the fluid acceleration conditional statistics are the same as in the entire domain. This observation can provide some help in studying the β and St dependence of the clustering morphology of the bubbles presented by Calzavarini *et al.* (2008).

Based on these observations, we propose, within the LES framework, an extension of the approach of Gorokhovski & Zamansky (2018) in order to account for the unresolved fluid turbulent fluctuations in the dynamics of micro-bubbles for locally homogenous and isotropic high-Reynolds numbers flows. To this end, the instantaneous acceleration of the bubble is decomposed into a filtered contribution given by the resolved fluid velocity field and a random contribution. The stochastic part is given by the sum of two correlated random processes, one for the drag forces

and the second for the fluid inertia terms. For the instantaneous norm of both forces, we consider the fluctuations of the energy transfer rate, relying on the fact that the fluctuations of the norm are self-similar for a given value of the energy transfer rate. For the latter a surrogate is obtained by a log-normal stochastic process evolving along the bubble trajectory. Whereas the former, which is observed to be invariant, is estimated from the variance of the forces conditioned on the dissipation rate as obtained from the model derived in this paper. The residual part is supplemented by a stochastic process for the orientations of the two forces. The model is given by two coupled random walks on the surface of the unit sphere, which enables us to reproduce the progressive decorrelation of the force components, their correlation with the large-scale motion, as well as the return to local isotropy for sufficiently large-scale separation, and the preferential anti-alignment of the two forces observed for $St < 1$. To summarize, the model depends on the Stokes number and the β parameter of the bubbles as well as a local Reynolds number Re_Δ based on the mesh size. In addition few parameters of the model need to be prescribed from the DNS.

The comparisons of the statistics obtained with LES supplemented by the proposed stochastic model with the ones obtained from DNS confirmed that the dynamics of the bubbles can be accurately computed by this approach even for very coarse meshes while the standard LES approach (without stochastic modelling for the high frequency fluctuations) fails to reproduce the statistics of the DNS. Nevertheless, the bubble clustering at subgrid scales or short-time relative dispersion are not improved by the modelling presented in this paper because the estimation of the dissipation rates along each bubble trajectory is obtained by independent stochastic processes.

The derivation of the proposed model is made for arbitrary density ratio, although, in this paper we only focus on the micro-bubble regime ($\beta = 3$). It can be shown that for $\beta = 0$ our model becomes equivalent to the formulation proposed for inertial particles in Gorokhovski & Zamansky (2018). Moreover, for neutrally dense particles ($\beta = 1$), the proposed model would provide results equivalent to those obtained for vanishingly small Stokes number, as expected for particles much smaller than the Kolmogorov scales. The assessment of the model for intermediate values of β is also interesting but is postponed for future work. Also interesting is to account for other forces that can have a non-negligible role on the bubble dynamics (buoyancy, lift and history). As well, accounting for the deformation of the bubbles is necessary if one is interested in bubbles larger than the micro-scale of the flow ($d_b > \eta$). Finally, we have focused on the modelling of the subgrid scale for homogenous and isotropic turbulent flow. Nevertheless, we think that the model proposed in this paper could provide acceptable results for flows that can be considered locally isotropic and homogenous at the scale of the mesh, since the main parameters of the model are defined locally.

REFERENCES

BEC, J., BIFERALE, L., BOFFETTA, G., CELANI, A., CENCINI, M., LANOTTE, A., MUSACCHIO, S. & TOSCHI, F. 2006 Acceleration statistics of heavy particles in turbulence. *J. Fluid Mech.* **550**, 349–358.

BEC, J., BIFERALE, L., CENCINI, M., LANOTTE, A. & TOSCHI, F. 2010 Intermittency in the velocity distribution of heavy particles in turbulence. *J. Fluid Mech.* **646**, 527–536.

BERROUK, A. S., LAURENCE, D., RILEY, J. J. & STOCK, D. E. 2007 Stochastic modelling of inertial particle dispersion by subgrid motion for les of high Reynolds number pipe flow. *J. Turbul.* **8**, N50.

BOS, W. J. T. & ZAMANSKY, R. 2019 Power fluctuations in turbulence. *Phys. Rev. Lett.* **122** (12), 124504.

BREUER, M. & HOPPE, F. 2017 Influence of a cost–efficient Langevin subgrid-scale model on the dispersed phase of large–eddy simulations of turbulent bubble–laden and particle–laden flows. *Intl J. Multiphase Flow* **89**, 23–44.

BURTON, G. C. & DAHM, W. J. A. 2005a Multifractal subgrid-scale modeling for large-eddy simulation. I. Model development and *a priori* testing. *Phys. Fluids* **17**, 075111.

BURTON, G. C. & DAHM, W. J. A. 2005b Multifractal subgrid-scale modeling for large-eddy simulation. II. Backscatter limiting and a posteriori evaluation. *Phys. Fluids* **17**, 075112.

CALZAVARINI, E., KERSCHER, M., LOHSE, D. & TOSCHI, F. 2008 Dimensionality and morphology of particle and bubble clusters in turbulent flow. *J. Fluid Mech.* **607**, 13–24.

CALZAVARINI, E., VOLK, R., BOURGOIN, M., LÉVÊQUE, E., PINTON, J.-F. & TOSCHI, F. 2009 Acceleration statistics of finite-sized particles in turbulent flow: the role of Faxén forces. *J. Fluid Mech.* **630**, 179–189.

CASTAING, B. 1996 The temperature of turbulent flows. *J. Phys. II* **6**, 105–114.

CASTAING, B., GAGNE, Y. & HOPFINGER, E. J. 1990 Velocity probability density functions of high Reynolds number turbulence. *Physica* D **46** (2), 177–200.

CHEN, S., DOOLEN, G. D., KRAICHNAN, R. H. & SHE, Z.-S. 1993 On statistical correlations between velocity increments and locally averaged dissipation in homogeneous turbulence. *Phys. Fluids* **5** (2), 458–463.

CLIMENT, E. & MAGNAUDET, J. 1999 Large-scale simulations of bubble-induced convection in a liquid layer. *Phys. Rev. Lett.* **82**, 4827–4830.

DHOTRE, M. T., DEEN, N. G., NICENO, B., KHAN, Z. & JOSHI, J. B. 2013 Large eddy simulation for dispersed bubbly flows: a review. *Intl J. Chem. Engng* **2013**, 343276.

FEDE, P. & SIMONIN, O. 2006 Numerical study of the subgrid fluid turbulence effects on the statistics of heavy colliding particles. *Phys. Fluids* **18** (4), 045103.

GATIGNOL, R. 1983 The Faxén formulae for a rigid particle in an unsteady non-uniform Stokes flow. *J. Méc. Théor. Appl.* **1**, 143–160.

GHATE, A. S. & LELE, S. K. 2017 Subfilter-scale enrichment of planetary boundary layer large eddy simulation using discrete fourier–gabor modes. *J. Fluid Mech.* **819**, 494–539.

GOROKHOVSKI, M. & ZAMANSKY, R. 2018 Modeling the effects of small turbulent scales on the drag force for particles below and above the Kolmogorov scale. *Phys. Rev. Fluids* **3** (3), 1–23.

VAN DEN HENGEL, E. I. V., DEEN, N. G. & KUIPERS, J. A. M. 2005 Application of coalescence and breakup models in a discrete bubble model for bubble columns. *Ind. Engng Chem. Res.* **44** (14), 5233–5245.

HINZE, J. O. 1975 *Turbulence*, 2nd edn. McGraw-Hill.

HU, G. & CELIK, I. 2008 Eulerian–Lagrangian based large-eddy simulation of a partially aerated flat bubble column. *Chem. Engng Sci.* **63** (1), 253–271.

JOHNSON, P. L. & MENEVEAU, C. 2017 Predicting viscous-range velocity gradient dynamics in large-eddy simulations of turbulence. *J. Fluid Mech.* **837**, 80–114.

KERSTEIN, A. R. 1999 One-dimensional turbulence: model formulation and application to homogeneous turbulence, shear flows, and buoyant stratified flows. *J. Fluid Mech.* **392**, 277–334.

KOLMOGOROV, A. N. 1941 The local structure of turbulence in incompressible viscous fluid for very large Reynolds numbers. *Dokl. Akad. Nauk SSSR* **434**, 9–13, translation by V. Levin 1991 *Phil. Trans. R. Soc. Lond.* A **434**, 9–13.

KOLMOGOROV, A. N. 1962 A refinement of previous hypotheses concerning the local structure of turbulence in a viscous incompressible fluid at high Reynolds number. *J. Fluid Mech.* **13**, 82–85.

LALESCU, C. C. & WILCZEK, M. 2018 Acceleration statistics of tracer particles in filtered turbulent fields. *J. Fluid Mech.* **847**, R2.

LANOTTE, A., CALZAVARINI, E., TOSCHI, F., BEC, J., BIFERALE, L. & CENCINI, M. 2011 Heavy particles in turbulent flows. International CFD Database, RM-2007-GRAD-2048.St0. iCFDdatabase.

LEGENDRE, D. & MAGNAUDET, J. 1997 A note on the lift force on a spherical bubble or drop in a low-Reynolds-number shear flow. *Phys. Fluids* **9** (11), 3572–3574.

LEGENDRE, D. & MAGNAUDET, J. 1998 The lift force on a spherical bubble in a viscous linear shear flow. *J. Fluid Mech.* **368**, 81–126.

LOISY, A. & NASO, A. 2017 Interaction between a large buoyant bubble and turbulence. *Phys. Rev. Fluids* **2**, 014606.

LUKASSEN, L. J. & WILCZEK, M. 2017 Lagrangian intermittency based on an ensemble of Gaussian velocity time series. In *Progress in Turbulence VII* (ed. R. Örlü, A. Talamelli, M. Oberlack & J. Peinke), pp. 23–29. Springer International Publishing.

MAGNAUDET, J. & EAMES, I. 2000 The motion of high-Reynolds-number bubbles in inhomogeneous flows. *Annu. Rev. Fluid Mech.* **32**, 659–708.

MATHAI, V., CALZAVARINI, E., BRONS, J., SUN, C. & LOHSE, D. 2016 Microbubbles and microparticles are not faithful tracers of turbulent acceleration. *Phys. Rev. Lett.* **117**, 024501.

MAXEY, M. R. & RILEY, J. J. 1983 Equation of motion for a small rigid sphere in a nonuniform flow. *Phys. Fluids* **26** (4), 883–889.

MAZZITELLI, I. M. & LOHSE, D. 2004 Lagrangian statistics for fluid particles and bubbles in turbulence. *New J. Phys.* **6** (1), 203.

MAZZITELLI, I. M., LOHSE, D. & TOSCHI, F. 2003 On the relevance of the lift force in bubbly turbulence. *J. Fluid Mech.* **488**, 283–313.

MENEVEAU, C. & KATZ, J. 2000 Scale-invariance and turbulence models for large-eddy simulation. *Annu. Rev. Fluid Mech.* **32**, 1–32.

MINIER, J.-P., CHIBBARO, S. & POPE, S. B. 2014 Guidelines for the formulation of Llagrangian stochastic models for particle simulations of single-phase and dispersed two-phase turbulent flows. *Phys. Fluids* **26**, 113303.

MORDANT, N., CRAWFORD, A. M. & BODENSCHATZ, E. 2004 Three-dimensional structure of the Lagrangian acceleration in turbulent flows. *Phys. Rev. Lett.* **93** (21), 214501.

MORDANT, N., METZ, P. & MICHEL, O. 2001 Measurement of Lagrangian velocity in fully developed turbulence. *Phys. Rev. Lett.* **21**, 214501.

PARK, G. I., BASSENNE, M., URZAY, J. & MOIN, P. 2017 A simple dynamic subgrid-scale model for les of particle-laden turbulence. *Phys. Rev. Fluids* **2** (4), 044301.

PEREIRA, R. M., MORICONI, L. & CHEVILLARD, L. 2018 A multifractal model for the velocity gradient dynamics in turbulent flows. *J. Fluid Mech.* **839**, 430–467.

POPE, S. B. 1990 Lagrangian microscales in turbulence. *Phil. Trans. R. Soc. Lond.* A **333** (1631), 309–319.

POPE, S. B. & CHEN, Y. L. 1990 The velocity-dissipation probability density function model for turbulent flows. *Phys. Fluids* **2** (8), 1437–1449.

POZORSKI, J. & APTE, S. V. 2009 Filtered particle tracking in isotropic turbulence and stochastic modeling of subgrid-scale dispersion. *Intl J. Multiphase Flow* **35** (2), 118–128.

PRAKASH, V. N. 2013 Light particles in turbulence. PhD thesis, University of Twente, Enschede.

PRAKASH, V. N., TAGAWA, Y., CALZAVARINI, E., MERCADO, J. M., TOSCHI, F., LOHSE, D. & SUN, C. 2012 How gravity and size affect the acceleration statistics of bubbles in turbulence. *New J. Phys.* **14** (10), 105017.

SABELNIKOV, V., BARGE, A. & GOROKHOVSKI, M. 2019 Stochastic modeling of fluid acceleration on residual scales and dynamics of suspended inertial particles in turbulence. *Phys. Rev. Fluids* **4** (4), 044301.

SABEL'NIKOV, V., CHTAB, A. & GOROKHOVSKI, M. 2007 The coupled LES – sub-grid stochastic acceleration model (LES-SSAM) of a high Reynolds number flows. In *Advances in Turbulence XI*, vol. 117, pp. 209–211; 11th EUROMECH European Turbulence Conference, June 25–28, 2007, Porto, Portugal: Springer Proceedings in Physics.

SABEL'NIKOV, V., CHTAB-DESPORTES, A. & GOROKHOVSKI, M. 2011 New sub-grid stochastic acceleration model in LES of high-Reynolds-number flows. *Eur. Phys. J.* B **80** (2), 177–187.

SAGAUT, P. 2002 *Large Eddy Simulation for Incompressible Flows: An Introduction*, 2nd edn. Springer.

SAWFORD, B. L. 1991 Reynolds number effects in Lagrangian stochastic models of turbulent dispersion. *Phys. Fluids* A **3**, 1577–1588.

SAWFORD, B. L. & GUEST, F. M. 1991 Lagrangian statistical simulation of the turbulent motion of heavy particles. *Boundary-Layer Meteorol.* **54** (1–2), 147–166.

SAWFORD, B. L. & YEUNG, P. K. 2011 Kolmogorov similarity scaling for one-particle Lagrangian statistics. *Phys. Fluids* **23** (9), 091704.

TAGAWA, Y., MERCADO, J. M., PRAKASH, V. N., CALZAVARINI, E., SUN, C. & LOHSE, D. 2012 Three-dimensional Lagrangian Voronoï analysis for clustering of particles and bubbles in turbulence. *J. Fluid Mech.* **693**, 201–215.

TAGAWA, Y., ROGHAIR, I., PRAKASH, V. N., VAN SINT ANNALAND, M., KUIPERS, H., SUN, C. & LOHSE, D. 2013 The clustering morphology of freely rising deformable bubbles. *J. Fluid Mech.* **721**, R2.

TCHEN, C. M. 1947 Mean value and correlation problems connected with the motion of small particles suspended in a turbulent fluid. PhD thesis, Delft University, Netherlands.

TENNEKES, H. & LUMLEY, J. L. 1972 *A First Course in Turbulence*. MIT Press.

VOLK, R., CALZAVARINI, E., VERHILLE, G., LOHSE, D., MORDANT, N., PINTON, J.-F. & TOSCHI, F. 2008a Acceleration of heavy and light particles in turbulence: comparison between experiments and direct numerical simulations. *Physica* D **237** (14–17), 2084–2089.

VOLK, R., MORDANT, N., VERHILLE, G. & PINTON, J.-F. 2008b Laser doppler measurement of inertial particle and bubble accelerations in turbulence. *Eur. Phys. Lett.* **81**, 34002.

YEUNG, P. K. 2001 Lagrangian characteristics of turbulence and scalar transport in direct numerical simulations. *J. Fluid Mech.* **427**, 241–274.

YEUNG, P. K., POPE, S. B., LAMORGESE, A. G. & DONZIS, D. A. 2006 Acceleration and dissipation statistics of numerically simulated isotropic turbulence. *Phys. Fluids* **18**, 065103.

ZAICHIK, L. I. & ALIPCHENKOV, V. M. 2011 A model for predicting the acceleration variance of arbitrary-density finite-size particles in isotropic turbulence. *Intl J. Multiphase Flow* **37** (3), 236–240.

ZAMANSKY, R., COLETTI, F., MASSOT, M. & MANI, A. 2016 Turbulent thermal convection driven by heated inertial particles. *J. Fluid Mech.* **809**, 390–437.

ZAMANSKY, R., VINKOVIC, I. & GOROKHOVSKI, M. 2013 Acceleration in turbulent channel flow: universalities in statistics, subgrid stochastic models and an application. *J. Fluid Mech.* **721**, 627–668.